Immune modulation and monitoring of cell therapy in inflammatory disorders

Suwandi, J.S.

Chapter 5.2

Tolerogenic dendritic cells pulsed with islet antigen induce long-term reduction in T-cell autoreactivity in type 1 diabetes patients

Tatjana Nikolic*, Jessica S. Suwandi*, Joris Wesselius, Sandra Laban, Nicole van der Zwan, Antoinette M. Joosten, Petra Sonneveld, Dick Mul, Henk-Jan Aanstoot, Jaap-Jan Zwaginga* and BartO. Roep*

*Contributed equally

Abstract

Restoration of immune tolerance may halt disease progression in autoimmune diseases. Tolerogenic dendritic cells (tolDC) inhibit antigen-specific proinflammatory T-cells, generate antigen-specific regulatory T-cells and promote IL-10 production *in vitro,* and thus provide/ are an appealing immunotherapeutic approach to intervene in autoimmune disease progression. A placebo-controlled, dose escalation phase 1 clinical trial in nine adult patients with long-standing type 1 diabetes (T1D) demonstrated safety and feasibility of two (prime-boost) vaccinations with proinsulin peptide pulsed tolDC. Immunoregulatory effects of tolDC were monitored by antigen-specific T-cell assays and mass flow cytometry. While major leukocyte subsets remained stable, $ICOS^+CCR4^+TIGIT^+$ Tregs increased after the priming with peptide-pulsed tolDC. $CD103^+$ tissue resident and $CCR6^+$ effector memory $CD4^+$ T-cells also increased in response to the first tolDC injection and declined thereafter below baseline levels with time. Strikingly, the tolDC-vaccine induced a profound and lasting decline in pre-existing $CD4^+$ and $CD8^+$ T-cell responses to the vaccine peptide and islet autoantigens, up to 3 years after tolDC therapy. Our data identify immune correlates of mechanistic efficacy of intradermally injected tolDC diminishing autoimmunity in T1D.

Introduction

Induction or restoration of immune tolerance is still the Holy Grail in transplantation, allergy and autoimmune diseases (1). In this respect, many efforts over the past decades were also directed to control the underlying autoimmune process in type 1 diabetes (T1D). Inhibition of beta-cell destruction and with it preservation or restoration of endogenous insulin production is indeed essential for physiological blood glucose control reducing the risk of diabetic complications (2). Ideally, an immune intervention should selectively target beta-cell directed autoimmunity, leaving the general immunity against, for instance, cancer and pathogens intact. However, although preclinical studies showed that vaccination with whole autoantigens, peptides or plasmids, administered orally, intra-nasally or parenterally, is safe (3-7), still little or temporary clinical benefits was observed (8).

Dendritic cells (DC) add flexibility to immune modulation while they not only present antigens of choice but also critically determine the quality and direction of T-cell activation combining antigen presentation with appropriate immunoregulating signals (9). When skewed towards a tolerogenic phenotype together with presentation of beta-cell autoantigens, DCs could initiate or activate a regulating immune response and dampen the existing immunity against these antigens. Indeed, our preclinical studies demonstrated mechanisms of action supporting these hypotheses. In humanized HLA-DR4-transgenic mice, proinsulin peptide-pulsed tolDC prevented and reversed induced autoimmunity to proinsulin that lasted upon subsequent challenges with the islet autoantigen (10). Human tolDC also regulate by eliminating $CD4^+$ and $CD8^+$ T-cells (11) and inducing antigen-specific Tregs (10, 12, 13). Tregs, in turn, change mature DC to become anti-inflammatory ('infectious tolerance') (12) and suppress immune responses to other islet autoantigens present on the same DC ('linked suppression') (12). These processes proved critically dependent on expression of PD-L1, membrane-bound TNF, ICOS-L, B7-H3 and the appropriate HLA on tolDC to allow antigen-specificity. TolDC-induced Tregs resemble induced antigen-specific Tr-1, *in vivo* circulating islet-specific Tregs as well as

(activated) thymic derived Tregs (tTregs) (14-16).

This regulation by tolDC of antigen-specific immune responses *in vitro* and previous observations that injecting naturally derived proinsulin peptide C19-A3 in humans is safe (7, 17, 18) prompted us to assess this peptide-cell combination for clinical intervention in T1D patients. After extensive preclinical characterization of tolDC production using a natural immunomodulator $1,25(OH)_2$vitaminD3 and dexamethasone and with it ensuring robust stability and quality (10-12, 19-22), these proinsulin-pulsed tolerance-inducing DCs were used in a recently completed phase 1 clinical trial. Nine patients with long standing T1D randomized into three groups each received one of the escalating doses ($0.5x10^7$, $1.0\ x10^7$ and $2.0\ x10^7$ cells) of proinsulin-pulsed tolDC by intradermal injections (23). One patient in each dosing group was first injected intradermally with saline (tolDC-vehicle) allowing monitoring of this placebo administration for three months prior to receiving peptide-pulsed tolDC injections in the respective dose. Safety and feasibility of this therapy was reported recently (23). Here, we report on mechanistic (immunological) efficacy of this approach to blunt islet autoimmunity. Building on our knowledge on their mechanisms of action of tolDC (24), we examined the immunological effect of tolDC treatment *in vivo* using various analyses measuring adaptive immunity and high-dimensional phenotyping of leukocyte subsets in peripheral blood.

Results

TolDC treatment modulates T-cell autoimmunity to the vaccine peptide

To determine whether autoreactive responses were modulated after tolDC treatment, we evaluated *ex vivo* T-cell proliferation and cytokine production upon antigen stimulation. Seven out of nine patients showed changes in islet autoimmunity upon injection with C19-A3 pulsed tolDC (Fig. 1). Patients are coded according to the received tolDC dosage and order of administration (p1-1 to p1-3 $0.5x10^7$ cells; p2-1 to p2-3 $1x10^7$ cells and p3-1 to p3-3 $2x10^7$ cells). T-cell autoimmunity to the vaccine peptide pre-existed before tolDC injection in three out of nine patients (p1-2, p1-3 and p3-3). Strikingly, all three responded to the tolDC therapy by reducing the proliferation (LST, Fig. 1A) and/or cytokine production (ELISPOT, Fig. 1B) to non-existing (cases p1-2 and p1-3) or IL-10 production alone (case p3-3) at the end of the 6-month study period. However, of the six patients not reacting to the vaccine peptide before tolDC therapy, an additional four showed a transient change in cytokine production (p1-1, p2-1, p2-3 and p3-2), with one patient (p2-3) attaining a moderate IL-10 producing phenotype at 6-month post-tolDC.

Next to the vaccine peptide, we measured autoreactive responses to preproinsulin protein (PPI) containing the vaccine peptide, and to other beta-cell autoantigens (GAD65, IA-2 and ZnT8; Fig. 2A, Fig. S1 and Fig. S2). Before tolDC administration, individual differences in proliferative response to autoantigens were noted in the frequencies of autoreactive PPI-specific $CD8^+$ T-cells and autoantibody titers (Fig. 2). Patients p1-2 p1-3 and p3-3 showed strong proliferative responses to PPI antigen (SI>10,) while patients p1-1, p2-3 and p3-3 had PPI-peptide specific $CD8^+$ T-cells before tolDC. Following tolDC administration, all patients presented with reduced values in both proliferative responses and frequencies of autoreactive $CD8^+$ T-cells. Autoantibody titers at the same time remained unaffected (Fig. 2) and neither did the responses to IA-2 and GAD65 prior to therapy change significantly by 6 months after tolDC therapy (Fig. S1) in 8 out of 9 patients. Patient p1-1 showed minimal proliferation

to control (TetTox) and beta-cell autoantigens prior to tolDC injection, which could reflect a refractory period of lymphocytes shortly after leukapheresis. Indeed, this patient subsequently showed increasing proliferation to all tested antigens including TetTox control. Of note, $CD8^+$ autoreactivity and autoantibody titers in this patient were similar before leukapheresis and after tolDC injection.

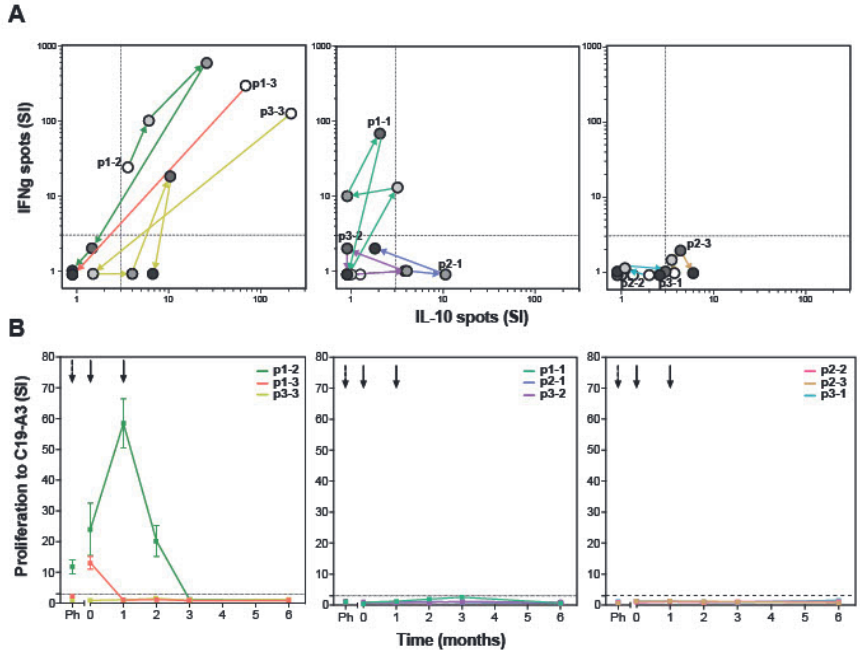

Fig. 1. TolDC therapy modulates T-cell responses to the vaccine peptide (C19-A3) (A) The C19-A3-specific T-cells producing cytokines IFNg and IL-10 were quantified using the ELISPOT assay. Left graph shows changes in IFNg/IL-10 production in three patients (p1-2, p1-3 and p3-3) with detectable cytokine responses to C19-A3 prior to tolDC therapy. Middle graph shows responses in three patients (p1-1, p2-1 and p3-2) with a temporary cytokine production to C19-A3 and right graph shows responses in three patients (p2-2, p2-3 and p3-1) with very low responses to C19-A3 prior and after tolDC therapy. For each patient, white circles show the number of cytokine-producing cells prior to tolDC treatment, successive circles with increasing grey tones depict 1, 2, 3 and 6 months post-tolDC therapy values. Patients are coded according to the received tolDC dosage (p1-1 to p1-3 $0.5x10^7$ cells; p2-1 to p2-3 $1x10^7$ cells and p3-1 to p3-3 $2x10^7$ cells). **(B)** Proliferative response to C19-A3 as determined by the lymphocyte stimulation test (LST). Proliferation was measured in triplicate as counts per minute (CPM) in wells with C19-A3 and % proliferation calculated as described in material and methods. Time of tolDC injections are indicated with black arrows.

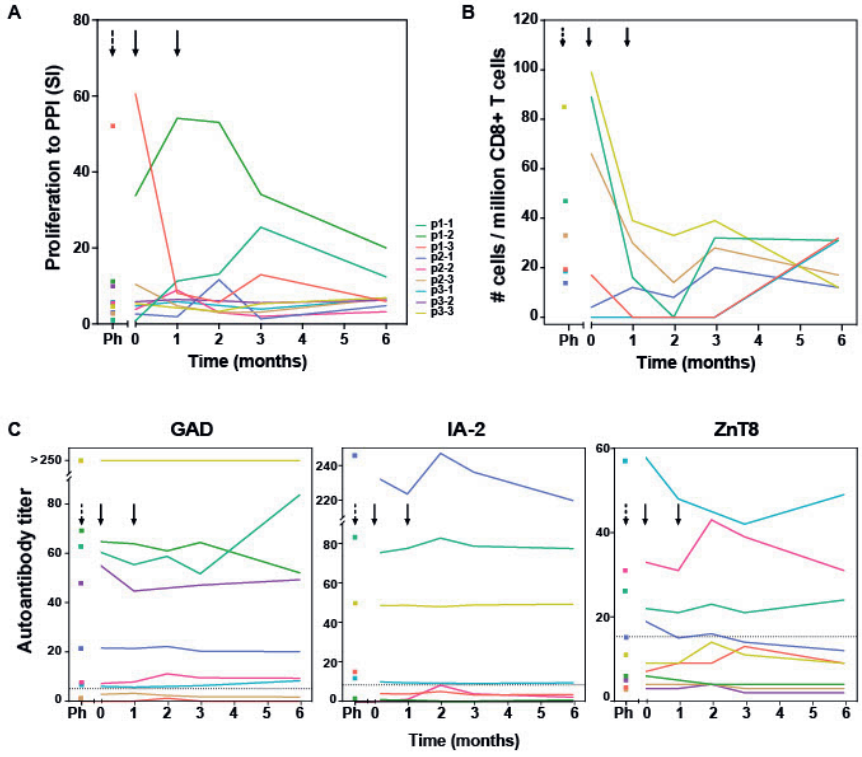

Fig. 2. Immunity to preproinsulin (PPI) and autoantibody titers up to 6 months after tolDC therapy. (A) Proinsulin reactive T-cells producing cytokines IFNg and IL-10 were quantified using the ELISPOT assay (left graph). Data are depicted as individual values (circles) and cumulated as violin plots with median, 25th and 75th percentile, prior to (0) and 6 months after tolDC therapy. Six out of nine patients show a reduction in PPI-specific IFNg and IL-10 spots after tolDC treatment. Right graphs show spaghetti plots of the proliferative response (LST) to PPI prior to leukapheresis (Ph), before tolDC (0) and at different time points after tolDC therapy for individual patients. **(B)** Quantification of $PPI_{9\text{-}24}$-specific $CD8^+$ T-cells using Q-dot assay prior to leukapheresis (Ph), before tolDC (0) and at different time points after tolDC therapy in six HLA-$A2^+$ patients. In three patients with the highest PPI-specific T-cell counts prior to therapy, reduction after tolDC therapy was observed, while low numbers of PPI-specific $CD8^+$ T-cells pre-treatment, remained low. **(C)** Autoantibody titers (GAD65, IA-2 and ZnT8) after tolDC treatment, show no changes i.e. signs of induction/increase in beta--cell autoimmunity. Lines represent individual patient titers. Values in the grey area are below the negative cut-off for that specific autoantibody. Titers too low to show in the graphs: for p1-3 GAD ≤ 1.2; for p1-2 IA-2 ≤ 0.8, for p2-3 and p3-2 IA-2 = 0.0.

Long-term modulation of T-cell responsiveness to PPI and diabetes control after tolDC

To investigate long-term effects of the tolDC therapy, patients were invited to participate in a single re-call visit (17-32 months after receiving the tolDC injections), at which point the responses to the vaccination peptide, PPI antigen and diabetes control were again assessed. Cytokine responses and proliferation to the vaccine peptide remained low or undetectable more than two years after the tolDC injection in all three patients (Fig. 3A-B). Moreover, also IFNg production to PPI was long-term decreased in all patients as compared to the levels before tolDC injection ($p=0.0016$; Fig. 3C) while IL-10 - although with individual variation- showed a decrease in most patients except for p1-3 and p2-1. The strong proliferation to PPI (SI > 10) before tolDC in the case of p1-2, p1-3 and p3-3 (Fig. 3D), decreased by 6 months after tolDC and persistently remained lower than before therapy. T-cell proliferation to other beta-cell antigens was also lower on the long term than at start in most patients (Fig. S1). Regarding glycaemic control, all participants had long-standing but well controlled T1D with HbA1c < 8% at start (range 6.4 – 7.6 %), which was maintained short term after tolDC therapy but clearly decreased on the long term by an average of 0.34% (range 6.2 – 7.3%, $p=0.0029$, ANOVA), in spite of constant insulin needs (Fig. 3E-F). Intriguingly, the HbA1c decline in some cases (p1-1, p2-1, p3-2, p3-3) resulted in personal 'all-time low' values, which was not always paired with the detectable maintained endogenous insulin production (p2-2, p2-3, p3-2), on the long term.

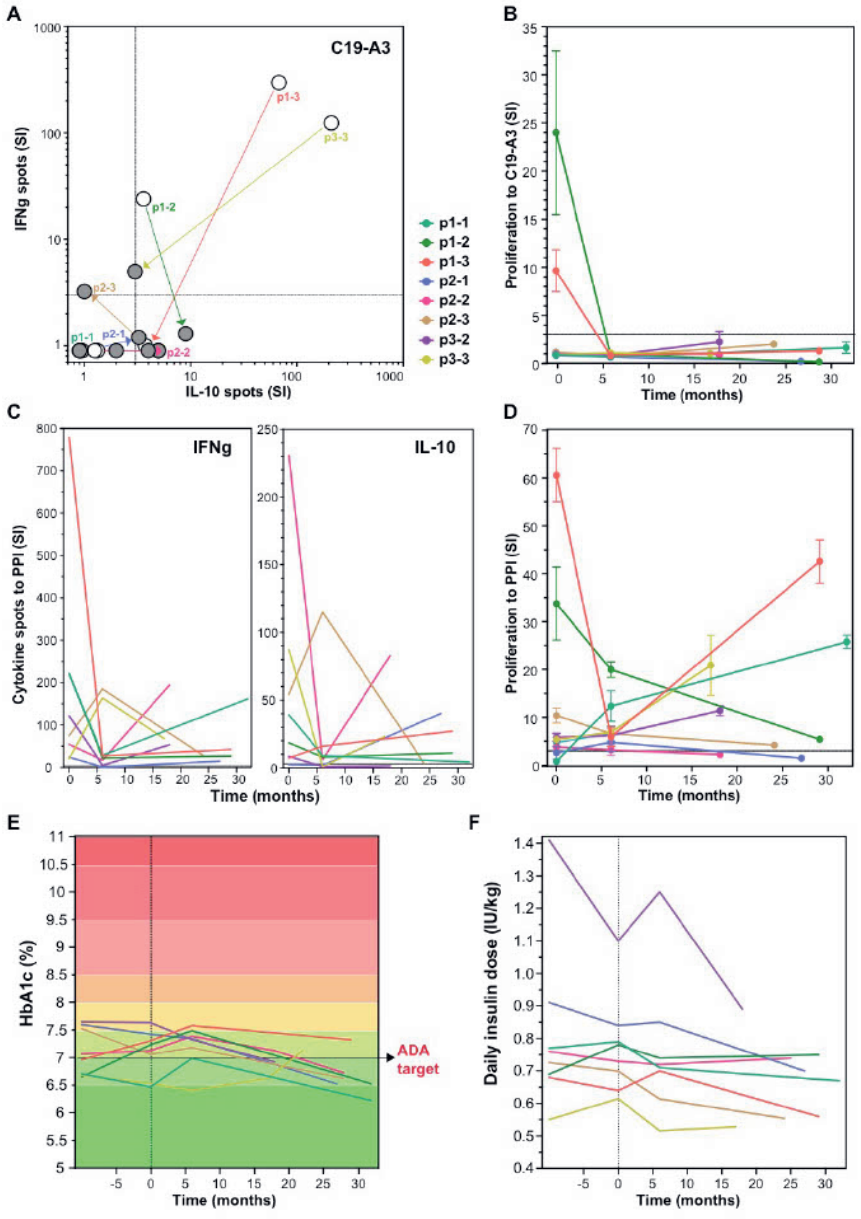

Fig. 3. Change in T-cell responses to C19-A3 vaccine peptide, preproinsulin (PPI) and glycemia control at long term (17-34 months) after tolDC therapy. Long-term effect of tolDC therapy on the cytokine response to C19-A3 **(A)** and PPI **(C)**. Patients reacting to C19-A3 prior to tolDC therapy, retain low response to C19-A3 at revisit and four out of eight patients show predominantly IL-10-producing response. TolDC therapy also reduced cytokine release to PPI with IFNg more strongly reduced than IL-10 in six out of eight patients at revisit (IFNg p=0.0012 and IL-10 p=0.34, paired T-test) . White dots depict the cytokine spots before tolDC and green dots at revisit. Patient specific values are connected. **(B)** and **(D)** Proliferation to C19-A3

peptide **(B)** and PPI **(D)** at revisit compared to the values before tolDC treatment. Lines represent individual patients coded in color as depicted. Patients p1-2, p1-3 and p2-1 reduced proliferation on the long term, other patients remain unchanged except for patient p1-1, showing an increased proliferation to PPI compared to the timepoint before tolDC therapy. **(E)** and **(F)** depict change in HbA1c and insulin use, respectively, at revisit.

TolDC do not affect general immune profiles

To assess the general immune competence after tolDC treatment, total white blood cell counts and the frequency of leukocyte subsets measured in full blood showed no systematic changes in total cell number or the frequency of leukocytes (B-cells, monocytes, DCs, NK cells, NKT cells, $CD4^+$ and $CD8^+$ T-cells; Fig. 4 and Fig. S3). Further gated subsets of B cells, monocytes, DC and NK cells in cryopreserved PBMC did not show significant changes post tolDC treatment either (Fig. S4). Important, antigen-specific immune competence unrelated to the vaccine peptide or general islet autoimmunity (proliferation to TetTox and virus-specific $CD8^+$ T-cell count did not change for patients either in the placebo period or post tolDC treatment (Fig. S1 and S2, respectively).

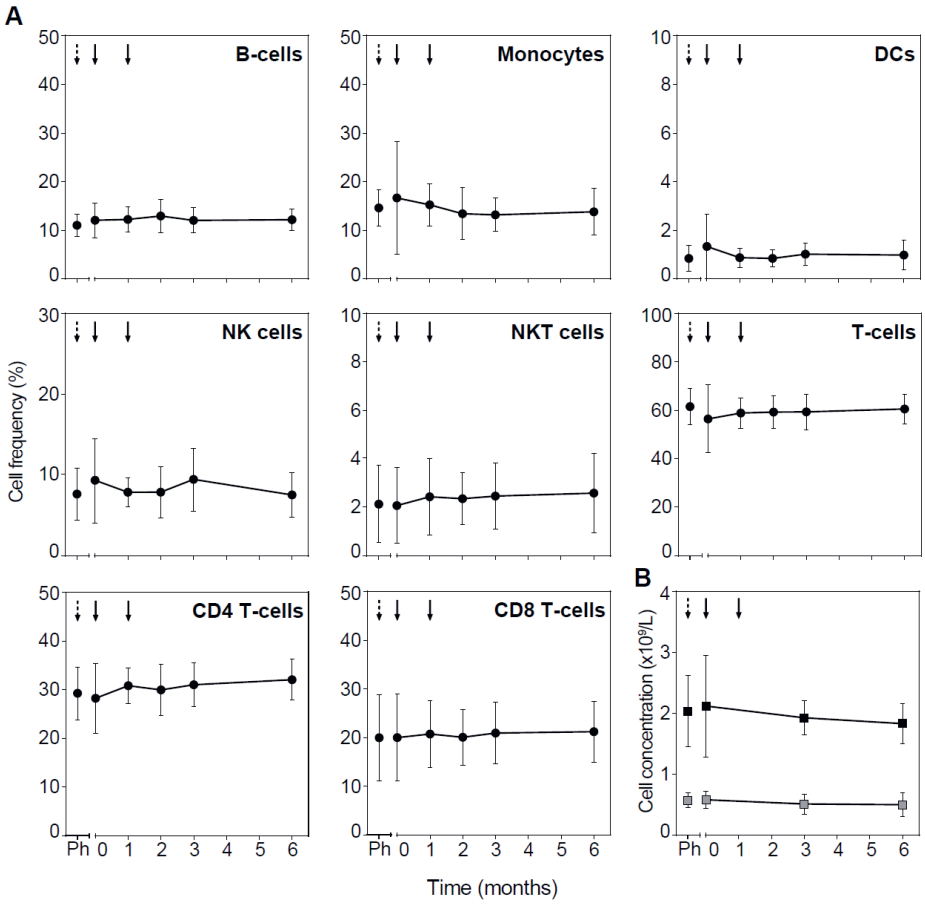

Fig. 4. TolDC treatment does not change PBMC subsets. (A) Frequency of leukocyte subsets determined in full blood by flow cytometry. Timepoint before leukapheresis is indicated with black dashed arrow (Ph) and tolDC treatment with black arrows. **(B)** Lymphocytes (black squares) and monocytes (grey squares) determined in absolute cell counts. Symbols represent the mean value ± SD of all patients. TolDC treatments are indicated with black arrows, dashed arrow (Ph) indicates timepoint before leukapheresis.

Mass cytometry reveals changes in CD4⁺ and CD8⁺ T-cell clusters after tolDC treatment

To further screen for more subtle changes in immune effector cells, frozen PBMC sampled at all monitoring timepoints were stained with a panel consisting of 39 lanthanide-conjugated antibodies and analyzed using Hierarchical Stochastic Neighbor Embedding (HSNE; Table S1). Confirming the results obtained from fresh blood, no significant changes were observed in total CD4**⁺**, CD8**⁺** and TCRγδ**⁺** T-cell populations prior to or after tolDC treatment (Fig. S5). Subsequent unsupervised HSNE analysis of the total CD4**⁺** T-cell population on the first level (level 1) allowed separation of seven major CD4-clusters based on the landmarks in the HSNE map (Fig. 5A), with designations based on the differential phenotype (Fig. 5B). While the cumulated frequencies of the clusters were similar between patients (Fig. 5C), three out of seven clusters changed frequency after the tolDC administration compared to baseline (cluster 1; p=0.012, cluster 4; p=0.007 and cluster 7; p=0.010, ANOVA). Cluster 1, with a phenotype of tissue resident memory T cells ($CD103^+$ Trm), showed an average increase of 0.13% (p=0.009) 1 month after the first tolDC injection and an increase of 0.10% 1 month after the second tolDC injection (p=0.047), both compared to baseline value (0.56% of total CD4**⁺** T cells), after which the frequencies normalized to baseline values (Fig. 5D, top graph). Cluster 4, consisting of naïve CD4**⁺** T-cells ($CD45RA^+CCR7^+$) dropped from baseline (46.2% of total CD4**⁺**) by 4.5% at 1 month after the first tolDC injection (p=0.012). After the second tolDC injection, the frequencies of cluster 4 returned to baseline values (Fig. 5D middle graph). Cluster 7, comprised of effector CD4**⁺** T-cells with a mixed central and effector memory (CM/EM) phenotype ($CD45RA^-CCR7^{dim}$), showed an increase in most patients with an average of 3.9% at 1 month after the first tolDC injection, which declined after the second tolDC injection in many patients below the baseline level (40.5% of total CD4**⁺**) and remained low until / or up to 6 months after the tolDC injection (Fig. 5D lower graph).

To further explore the tolDC-induced changes, next level CD4$^+$ T-cell cluster analysis was performed (level 2) (Fig. 5E) of the first level cluster 1, 4, 7 and additionally cluster 6. Within the first level Trm cluster 1, only subcluster 1.3 demonstrated significant change (p=0.0003), though all Trm subclusters showed a peak in frequency after the first tolDC injection (Fig. S6A). Within the CM/EM cluster 7, especially subclusters 7.1-7.4 sharing expression of CCR6 showed significant changes after tolDC injection (p=0.0003, p=0.003, p=0.0006 and p=0.001, respectively) (Fig. 5E and Fig. S6B). Though the percentage of cluster 6 did not change after tolDC injection at first level analysis, it was additionally studied because of its cells with a CD25^{high}CD127$^-$ phenotype and thus likely including both thymic derived Tregs as well as peripherally induced Tregs (25, 26). In our level 2 analyses, this cluster divided into four subclusters (6-1 to 6-4) (Fig. 5E). Based on phenotype and a pseudotime analysis, diverging Treg subclusters could be determined by differential marker expression (Fig. 6) that likely represented naïve Tregs expressing CD45RA (subcluster 6-1 and 6-2), an intermediate cluster described in the literature as Fraction III (27) and activated effector Tregs (eTregs; subcluster 6-4) expressing TIGIT, ICOS, CD39 and CCR4 (Fig. 6A-B and Fig. S7)., Indeed a shift in the subclusters balance from naïve and Fr. III Tregs towards eTregs (subcluster 6-4) was evident starting 1 month after the first tolDC injection with 2.72% eTregs at baseline increasing on average by 0.49% (p=0.035) at the cost of the other subclusters (Fig. 6C).

Similar HSNE analysis but of the CD8$^+$ T-cell compartment revealed eight major clusters (level 1) (Fig. S8A-C). Significant change was detected in cluster 7 (p=0.042), representing CD8$^+$ T-cells with a memory phenotype (CD45RA$^-$CCR7^{dim}) expressing CD25^{dim} and a skin-tropic molecule CCR4 (Fig. S8D). One month after the first tolDC injection, a slight increase of 0.75% of CD8$^+$ (p=0.0029) was observed, which normalized to baseline values (4.45% of total CD8$^+$) after the second tolDC injection. Within cluster 7, we found that subcluster 7.3 expressing KLRG1 associated with T-cell senescence (28), significantly increased after tolDC injection (p=0.022). Subclusters

7.1, 7.4 and 7.7 sharing low expression of CD25 but negative for KLRG1, also showed a peak in frequency 1 month after the first injection (Fig. S8F).

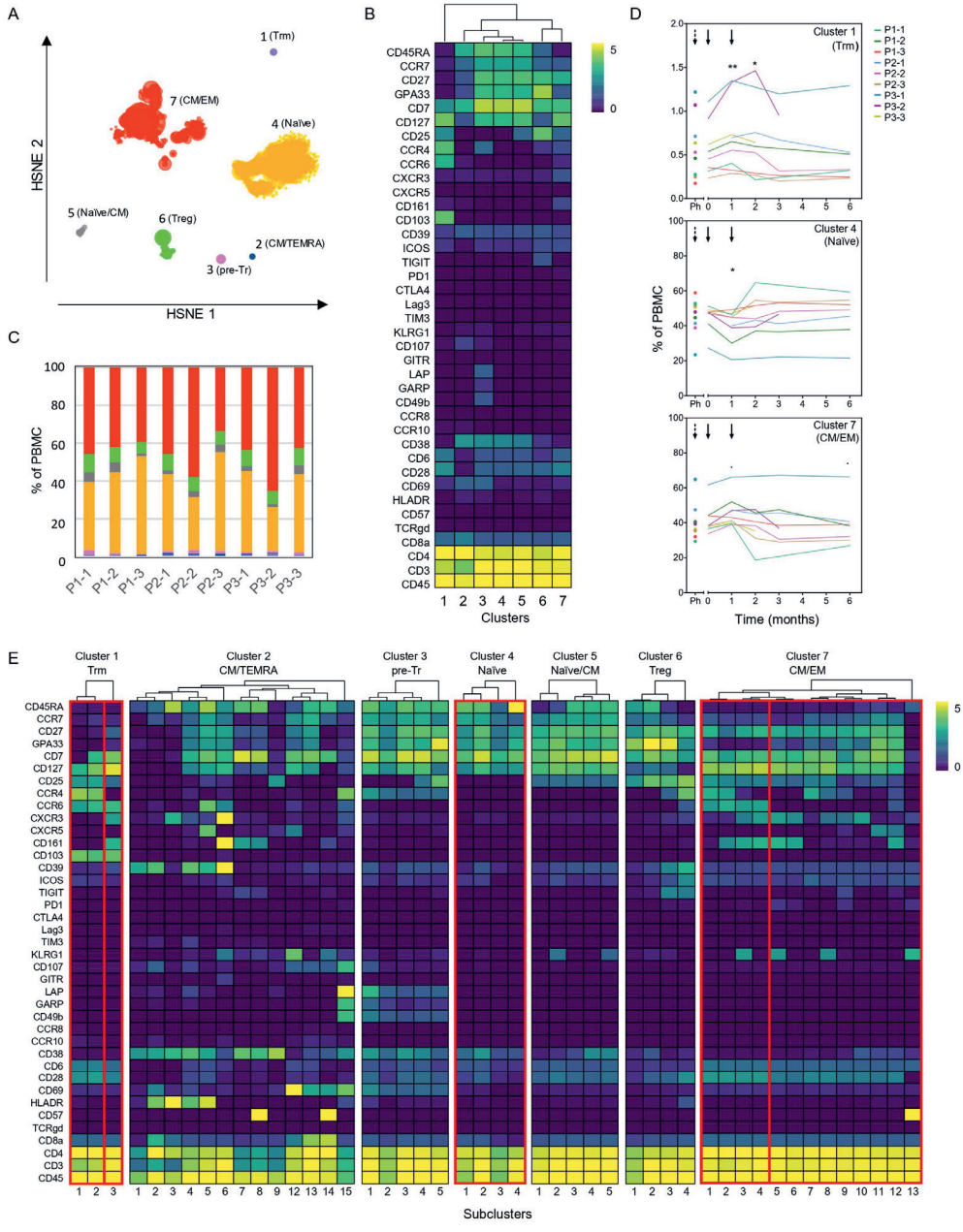

Fig. 5. High dimensional analysis of the CD4$^+$ T-cell compartment reveals changes after tolDC treatment. Analysis of CD4$^+$ T-cells from tolDC-treated patients containing multiple timepoints before and after tolDC treatment (n=9). **(A)** HSNE analysis reveals seven major CD4$^+$ T-cell clusters at the overview level (level 1). **(B)** Clustered heatmap displays the phenotype of major clusters. **(C)** Distribution of major clusters within each patient (all timepoints combined). Colors correspond to the HSNE map in A. **(D)** Line plots display frequency of clusters for individual patients in time. The frequency in clusters 1, 4 and 7 significantly changed after tolDC treatment (cluster 1; p=0.012, cluster 4; p=0.007 and cluster 7; p=0.010). Black arrows show time of first and second tolDC injection, dashed arrows indicate the timepoint before leukapheresis. Each line represents one patient. **(E)** The heterogeneity within each major cluster is further explored in a new HSNE analysis (level 2). Generated subclusters are visualized in a heatmap. Boxes indicate significant major- and subclusters. Lineplots of significant subclusters are displayed in Fig. S5.

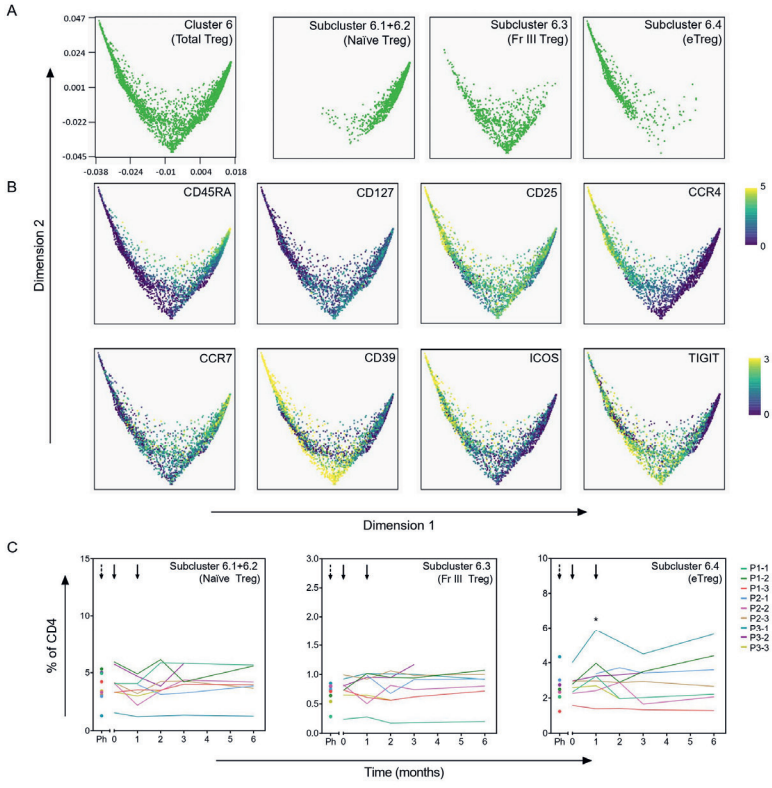

Fig. 6. Effect of tolDC on regulatory T-cell subsets. Pseudotime analysis (diffusion map) shows differentiation trajectory within Treg cluster 6. **(A)** Treg subclusters as defined in Cytosplore (Fig. 5E) are visualized in the diffusion map. Subclusters 6.1 and 6.2 are plotted together since both subclusters show a naïve phenotype. **(B)** Specified markers within the diffusion map. **(C)** Frequency in time of total Treg and Treg subclusters, shows significant increase of eTregs (subcluster 6.4) 1 month after tolDC treatment (p=0.035).

Discussion

Elaborating on the safety and feasibility of tolDC therapy established in a phase 1 placebo controlled, dose escalation study, we here describe the first outcomes on immunological efficacy in our patients with long standing T1D (23). Notwithstanding the limited size of a safety trial, first evidence revealed itself of antigen-pulsed tolDC modulation of autoimmunity *in vivo*, predominantly targeting $CD4^+$ T-cell responses and sparing general immune reactivity. Prime-boost intradermal injections of tolDC selectively stimulated T-cells, including a subset of Tregs, and reduced the frequency of $CCR6^+$ effector $CD4^+$ T-cells, leaving all other peripheral blood cells unchanged. Furthermore, we found evidence of long-term antigen-specific immunological tolerance induced by tolDC in all patients with pre-existing vaccine-specific T-cell responses. Analyses of the autoimmunity more than two years after tolDC administration in a post-hoc patient revisit furthermore confirmed a long-lasting reduction in effector immune responses to the vaccine-peptide that in some cases extended to the whole PPI antigen. Patients also presented with long-term stable (three patients) or improved glycaemic control (five patients) in spite of similar or slightly reduced insulin need, compared to a 6–9-month average monitoring period before the tolDC injection. While we have no definitive profile that these 'all-time low' HbA1c values are a direct consequence of immunotherapy, the shown superior glycaemic control given the long disease duration beyond diagnosis should be considered at least one of the strongest possible safety confirmations of our therapy.

Adding to the observed antigen- specific immune-modulation by tolDCs, high-dimensional phenotypic analysis of PBMC enabled assessment of numerous T-cell subsets, next to adaptive T-cell responses. TolDC vaccination increased a particular Treg subset *in vivo* resembling Tregs with strong suppressive capacity induced by tolDC *in vitro* (expressing CD25, CCR4, ICOS and HLA-DR) (16). TolDC therapy was also followed by a transient increase of Trm $CD4^+$ T-cells expressing CD103 (29). Trm cells can exit the tissue and re-enter the circulation (30). This transient increase might in

this respect reflect the response of skin-residing Trm to the intradermally injected tolDCs, and indeed two patients receiving the highest tolDC dose (p3-1 and p3-2) showed the highest increase in Trm T-cells in the blood. Most pronounced changes were observed for $CCR6^+$ effector $CD4^+$ T-cells that initially increased but then declined at 6 months after tolDC therapy to frequencies below baseline values. TolDC induce antigen-specific apoptosis of effector $CD4^+$ T-cells (10, 16, 21, 24). Within this declining effector T-cell pool, $CCR6^+$ cells co-expressed CCR4 (subclusters 7.1 and 7.2) or CXCR3 (subclusters 7.3 and 7.4), indicating that both levels of Th17- and Th1-like Th17 cells may be reduced by tolDC therapy, both of which have been proposed to play a role in islet destruction and T1D (31-33) (34, 35). Monitoring of beta cell specific autoimmunity by proliferation and ELISPOT analyses indeed likewise suggest that circulating effector T cells reactive to proinsulin peptide disappeared or became IL-10 producing. Moreover, the latter persisted long after tolDC therapy in patients that showed pre-existing response (p1-2, p1-3, p3-3) and in an additional four patients, in which tolDC induced temporary immunity to the vaccine peptide (p1-1, p2-1, p2-3, p3-2). While our observations in seven out of nine patients support that tolDC induce some form of immune tolerance to the vaccine peptide *in vivo*.

TolDC therapy did not induce general changes within the $CD8^+$ T-cell compartment with only a transient and moderate increase of one cluster (cluster 7; $CD25^{dim}$ memory $CD8^+$ T-cells), a heterogeneous subset containing cells with phenotypes of skin-homing, senescent, and early effector $CD8^+$ T-cells (36) was observed. This would be consistent that pulsing tolDC with a peptide eluted from HLA-DR4 (37) likely target the $CD4^+$ T-cell compartment. Nonetheless, a specific and long-standing reduction of autoreactive $CD8^+$ T-cells was observed while the number of virus-specific $CD8^+$ as proxy for general CD8 functionality remained unaffected. In addition, the *ex vivo* proliferative response to other beta-cell antigens declined in time, suggestive of tolDC mediated so called linked suppression broadened to other islet-specific responses, reflected by increased levels of induced Tregs. These observations are not definitive

but at least show to test the infectious tolerance *in vivo,* as tolDC were demonstrated to induce *in vitro* (12).

By its design, our limited phase 1 trial in long standing T1D precluded assessment of tolDC's clinical efficacy to preserve beta-cell function. Yet, our findings not only confirm safety by stable blood leukocyte subsets and preserved non-vaccine related immune responses but encouraging, selective modulation of relevant T cell subsets and a long-lasting annihilation of pre-existent vaccine-specific responses after the tolDC treatment in combination with exceptional and unprecedented glycaemic control. TolDC therapy therefore seems able to adjust the immune system towards autoantigen-specific tolerance *in vivo.* This in our opinion, justifies further clinical testing of proinsulin-pulsed tolDC to induce long-lasting specific immune modulation in T1D patients with still remaining beta-cell function. Such trials will establish whether beta-cells eventually can be protected from autoimmune destruction.

Materials and Methods

Study design, in vitro generation and administration of clinical grade tolDC

The clinical study protocol was approved by the Dutch Central Committee on Research Involving Human Subjects and the Medical Ethical Committee of Leiden University Medical Center (LUMC; Leiden, The Netherlands), EudraCT number 2013-005476-18. Patients were selected for screening by their own physician at Diabeter clinic (The Netherlands). Nine patients eligible for the study and willing to participate were allocated at random to a dose treatment group: $0.5x10^7$ (p1-1, p1-2 and p1-3), $1x10^7$ (p2-1, p2-2 and p2-3) or $2x10^7$ (p3-1, p3-2 and p3-3) tolDCs per injection (23). A randomly selected patient in each dose-cohort first received 5, 10 or 20 intradermal injections of saline (the tolDC vehicle), respectively. In this 'placebo' period, participants were monitored for three months (12 weeks), after which they received tolDC injections and were monitored as a third participant in their respective dose-group. Detailed description of clinical tolDC generation and quality assessment has been reported (23). TolDCs were administered by intradermal injection in the upper-left abdominal quadrant, using a MicronJet600 microneedle (NanoPass Technologies Ltd, Nes Ziona, Israel), at the Clinical Cellular Research Unit of the Hemapheresis Unit (LUMC). (23).

Immunomonitoring

The monitoring schedule included participants visit to LUMC at one, two, three and six months after the first tolDC administration. For the long-term analyses, study participants were invited for re-analyses in June 2019, which represented 17-34 months after the first tolDC injection. Blood samples were taken for immunomonitoring, hematology and chemistry analyses and HbA1c measurement. Antigen-specific immunomonitoring was performed using techniques previously validated for clinical trials: fresh PBMCs were cultured with GMP-grade C19-A3 peptide, or PPI protein to detect antigen-specific IFN-g and IL-10 producing cells using ELISPOT assay (17); antigen-specific proliferation was assessed in the lymphocyte

stimulation test (LST) (38, 39). In short, fresh PBMC were incubated with GMP-grade C19-A3 peptide, recombinant human proteins PPI, GAD65 and IA-2 (all at final conc. 10 µg/mL), synthesized at the Protein Facility (LUMC). For control, cells were incubated with medium alone (med), tetanus toxoid (1%, 7.23 Lf/mL; Statens Serum Institut) or recombinant IL-2 (Proleukin®, 35 U/mL; Novartis, Bazel, Switzerland). For the linked-response analyses, fresh PBMC were incubated with protein antigens together with vaccine peptide C19-A3. To quantify PPI-specific $CD8^+$ autoreactive T-cells, the Q-dot assay was performed using frozen PBMC as described and validated previously (7, 40).

Autoantibody titers for glutamic acid decarboxylase antibody (GADA), insulinoma-associated antigen-2 antibody (IA-2A) and zinc transporter 8 antibody (ZnT8A) were determined from serum (at least 0.5 mL per sample) by commercial ELISA at the Laboratory for Medical Immunology Reinier de Graaf (Delft, The Netherlands).

Flow cytometry of fresh whole blood and cryopreserved PBMC

The flow cytometric analysis of whole blood was designed following reported protocols of the ONE study and Immune tolerance network (ITN) (41, 42). In short, 1 mL freshly drawn, heparinized peripheral blood was washed three times with washing buffer (PBS with 2% FCS (Sigma-Aldrich), to remove blood components that interfere with antibody binding. Washed blood was incubated with a titrated cocktail of antibodies for 15 minutes in the dark at room temperature (Table S1). Subsequently, lysing buffer (BD Biosciences) was added for 10 minutes (dark, room temperature) and washed thereafter with FACS buffer. Samples were kept in stabilizing fixation buffer (BD Biosciences) until acquisition within 48 hours using FACS Canto II (BD Biosciences). For additional flow cytometric analysis, cryopreserved PBMC were thawed, washed with FACS buffer and stained with antibodies diluted in brilliant stain buffer for 45 minutes at room temperature (Table S1). Samples were kept in stabilizing fixation buffer (BD Biosciences) and were acquired within 48 hours using FACS LSR II (BD Biosciences).

Mass cytometry analyses

Cryopreserved PBMC used for the CyTOF analysis were were stained with a panel consisting of 39 metal-conjugated antibodies (Table S2) as described previously (43). To minimize inter-assay variability, samples of different timepoints from the same patient were stained and acquired on the same day and a reference sample was included as quality control. The reference sample consisted of 1,5% PHA stimulated PBMC from a healthy donor. To check the consistency between staining and measurement days, reference samples were analysed in a tSNE using Cytosplore and Jensen-Shannon plots were generated in Matlab (version R2016a) (Fig. S5C).

Statistical analysis

Proliferation in LST was tested using 2-way ANOVA and Dunnet's multiple comparison test. Changes in ELISPOT were tested using Wilcoxons matched-pairs signed rank test. Flow cytometric analyses were performed using FlowJo software (Ashland, OR, USA), linear mixed models were applied including patients as random effect and timepoints after tolDC injections as fixed effects. Principal component analysis was performed using R (package 3.5.2, 'ggplot2'). Graphs and statistical calculations were performed using GraphPad software (San Diego, CA, USA). Values at $p<0.05$ after multiple testing correction were deemed significant.

Data obtained by CyTOF were analysed as follows: Beads were excluded from the dataset and live, $CD45^+$ single cells were selected with DNA stains and Gaussian parameters (width and residual) (Fig. S5A) in FlowJo. Expression values were arcsine transformed and Hierarchical Stochastic Neighbor Embedding (HSNE) implemented in Cytosplore (version 2.2.1) (44) was used for dimensionality reduction analysis. The dataset was explored in different levels of hierarchies as described in the results section. Subsequent clusters were generated using the Gaussian-mean-shift method (Fig. S5B). FCS files from generated clusters were exported and loaded in R (version 3.6.2) using the "Cytofast" package (45) for further downstream analysis. A mixed linear model was used to evaluate changes in cell frequency of specific clusters after

tolDC treatment. Cell frequencies were compared with the baseline frequency at timepoint 0, before the first tolDC injection. The cell frequency of the cluster is selected as dependent variable, timepoints after tolDC injections are the fixed effects and the random effects are the different patients. An anova test was used to assess whether overall changes are observed in a cluster after tolDC treatment and p-values below 0.05 were considered statistically significant. Estimates of fixed effects from the mixed linear model are reported in the results as change in % of $CD4^+$ or $CD8^+$ T-cells. Statistical tests were performed using R package "lmerTest". Diffusion maps were generated in the OMIQ Data Science Platform using the Wanderlust function.

References

1. Roep BO, Wheeler DCS, Peakman M. Antigen-based immune modulation therapy for type 1 diabetes: the era of precision medicine. Lancet Diabetes Endocrinol. 2019;7(1):65-74.
2. Atkinson MA, Roep BO, Posgai A, Wheeler DCS, Peakman M. The challenge of modulating beta-cell autoimmunity in type 1 diabetes. Lancet Diabetes Endocrinol. 2019;7(1):52-64.
3. Larche M, Wraith DC. Peptide-based therapeutic vaccines for allergic and autoimmune diseases. Nature medicine. 2005;11(4 Suppl):S69-76.
4. Peakman M, Dayan CM. Antigen-specific immunotherapy for autoimmune disease: fighting fire with fire? Immunology. 2001;104(4):361-6.
5. Tian J, Kaufman DL. Antigen-based therapy for the treatment of type 1 diabetes. Diabetes. 2009;58(9):1939-46.
6. Alhadj Ali M, Liu YF, Arif S, Tatovic D, Shariff H, Gibson VB, et al. Metabolic and immune effects of immunotherapy with proinsulin peptide in human new-onset type 1 diabetes. Sci Transl Med. 2017;9(402).
7. Roep BO, Solvason N, Gottlieb PA, Abreu JR, Harrison LC, Eisenbarth GS, et al. Plasmid-encoded proinsulin preserves C-peptide while specifically reducing proinsulin-specific CD8(+) T cells in type 1 diabetes. Sci Transl Med. 2013;5(191):191ra82.
8. Staeva-Vieira T, Peakman M, von Herrath M. Translational mini-review series on type 1 diabetes: Immune-based therapeutic approaches for type 1 diabetes. Clinical and experimental immunology. 2007;148(1):17-31.
9. Figdor CG, de Vries IJ, Lesterhuis WJ, Melief CJ. Dendritic cell immunotherapy: mapping the way. Nature medicine. 2004;10(5):475-80.
10. Gibson VB, Nikolic T, Pearce VQ, Demengeot J, Roep BO, Peakman M. Proinsulin multi-peptide immunotherapy induces antigen-specific regulatory T cells and limits autoimmunity in a humanized model. Clinical and experimental immunology. 2015;182(3):251-60.
11. Kleijwegt FS, Jansen DT, Teeler J, Joosten AM, Laban S, Nikolic T, et al. Tolerogenic dendritic cells impede priming of naive CD8(+) T cells and deplete memory CD8(+) T cells. European journal of immunology. 2013;43(1):85-92.
12. Kleijwegt FS, Laban S, Duinkerken G, Joosten AM, Koeleman BP, Nikolic T, et al. Transfer of regulatory properties from tolerogenic to proinflammatory dendritic cells via induced autoreactive regulatory T cells. JImmunol. 2011;187(12):6357-64.
13. Beringer DX, Kleijwegt FS, Wiede F, van der Slik AR, Loh KL, Petersen J, et al. T cell receptor reversed polarity recognition of a self-antigen major histocompatibility complex. Nat Immunol. 2015;16(11):1153-61.
14. Tree TI, Lawson J, Edwards H, Skowera A, Arif S, Roep BO, et al. Naturally arising human CD4 T-cells that recognize islet autoantigens and secrete interleukin-10 regulate proinflammatory T-cell responses via linked suppression. Diabetes. 2010;59(6):1451-60.
15. Roncarolo MG, Battaglia M. Regulatory T-cell immunotherapy for tolerance to self antigens and alloantigens in humans. Nat Rev Immunol. 2007;7(8):585-98.
16. Suwandi JS, Laban S, Vass K, Joosten A, van Unen V, Lelieveldt BPF, et al. Multidimensional analyses of proinsulin peptide-specific regulatory T cells induced by tolerogenic dendritic cells. J Autoimmun. 2020;107:102361.
17. Arif S, Tree TI, Astill TP, Tremble JM, Bishop AJ, Dayan CM, et al. Autoreactive T cell responses show proinflammatory polarization in diabetes but a regulatory phenotype in health. JClinInvest. 2004;113(3):451-63.
18. Thrower SL, James L, Hall W, Green KM, Arif S, Allen JS, et al. Proinsulin peptide immunotherapy in type 1 diabetes: report of a first-in-man Phase I safety study. Clinical and experimental immunology. 2009;155(2):156-65.
19. Ferreira GB, Kleijwegt FS, Waelkens E, Lage K, Nikolic T, Hansen DA, et al. Differential protein pathways in 1,25-dihydroxyvitamin d(3) and dexamethasone modulated tolerogenic human dendritic cells. JProteomeRes. 2012;11(2):941-71.
20. Nikolic T, Roep BO. Regulatory multitasking of tolerogenic dendritic cells - lessons taken from vitamin d3-treated tolerogenic dendritic cells. Frontiers in immunology. 2013;4:113.

21. Unger WW, Laban S, Kleijwegt FS, van der Slik AR, Roep BO. Induction of Treg by monocyte-derived DC modulated by vitamin D3 or dexamethasone: differential role for PD-L1. EurJImmunol. 2009;39(11):3147-59.
22. van Halteren AG, Tysma OM, van EE, Mathieu C, Roep BO. 1alpha,25-dihydroxyvitamin D3 or analogue treated dendritic cells modulate human autoreactive T cells via the selective induction of apoptosis. JAutoimmun. 2004;23(3):233-9.
23. Nikolic T, Zwaginga JJ, Uitbeijerse BS, Woittiez NJ, de Koning EJ, Aanstoot HJ, et al. Safety and feasibility of intradermal injection with tolerogenic dendritic cells pulsed with proinsulin peptide-for type 1 diabetes. Lancet Diabetes Endocrinol. 2020;8(6):470-2.
24. Suwandi JS, Nikolic T, Roep BO. Translating Mechanism of Regulatory Action of Tolerogenic Dendritic Cells to Monitoring Endpoints in Clinical Trials. Frontiers in immunology. 2017;8:1598.
25. Adeegbe DO, Nishikawa H. Natural and induced T regulatory cells in cancer. Frontiers in immunology. 2013;4:190.
26. Povoleri GA, Scotta C, Nova-Lamperti EA, John S, Lombardi G, Afzali B. Thymic versus induced regulatory T cells - who regulates the regulators? Frontiers in immunology. 2013;4:169.
27. Togashi Y, Shitara K, Nishikawa H. Regulatory T cells in cancer immunosuppression - implications for anticancer therapy. Nat Rev Clin Oncol. 2019;16(6):356-71.
28. Wherry EJ, Kurachi M. Molecular and cellular insights into T cell exhaustion. Nat Rev Immunol. 2015;15(8):486-99.
29. Schenkel JM, Masopust D. Tissue-resident memory T cells. Immunity. 2014;41(6):886-97.
30. Klicznik MM, Morawski PA, Hollbacher B, Varkhande SR, Motley SJ, Kuri-Cervantes L, et al. Human CD4(+)CD103(+) cutaneous resident memory T cells are found in the circulation of healthy individuals. Sci Immunol. 2019;4(37).
31. Li M, Song LJ, Qin XY. Advances in the cellular immunological pathogenesis of type 1 diabetes. J Cell Mol Med. 2014;18(5):749-58.
32. Li Y, Liu Y, Chu CQ. Th17 Cells in Type 1 Diabetes: Role in the Pathogenesis and Regulation by Gut Microbiome. Mediators Inflamm. 2015;2015:638470.
33. Solt LA, Burris TP. Th17 cells in Type 1 diabetes: a future perspective. Diabetes Manag (Lond). 2015;5(4):247-50.
34. Honkanen J, Nieminen JK, Gao R, Luopajarvi K, Salo HM, Ilonen J, et al. IL-17 immunity in human type 1 diabetes. J Immunol. 2010;185(3):1959-67.
35. Potzl J, Botteron C, Tausch E, Pedre X, Mueller AM, Mannel DN, et al. Tracing functional antigen-specific CCR6 Th17 cells after vaccination. PLoS One. 2008;3(8):e2951.
36. Herndler-Brandstetter D, Schwaiger S, Veel E, Fehrer C, Cioca DP, Almanzar G, et al. CD25-expressing CD8+ T cells are potent memory cells in old age. J Immunol. 2005;175(3):1566-74.
37. Arif S, Tree TI, Astill TP, Tremble JM, Bishop AJ, Dayan CM, et al. Autoreactive T cell responses show proinflammatory polarization in diabetes but a regulatory phenotype in health. J Clin Invest. 2004;113(3):451-63.
38. Hilbrands R, Huurman VA, Gillard P, Velthuis JH, De WM, Mathieu C, et al. Differences in baseline lymphocyte counts and autoreactivity are associated with differences in outcome of islet cell transplantation in type 1 diabetic patients. Diabetes. 2009;58(10):2267-76.
39. Roep BO, Kallan AA, Duinkerken G, Arden SD, Hutton JC, Bruining GJ, et al. T-cell reactivity to beta-cell membrane antigens associated with beta-cell destruction in IDDM. Diabetes. 1995;44(3):278-83.
40. Velthuis JH, Unger WW, Abreu JR, Duinkerken G, Franken K, Peakman M, et al. Simultaneous detection of circulating autoreactive CD8+ T-cells specific for different islet cell-associated epitopes using combinatorial MHC multimers. Diabetes. 2010;59(7):1721-30.
41. van Unen V, Li N, Molendijk I, Temurhan M, Hollt T, van der Meulen-de Jong AE, et al. Mass Cytometry of the Human Mucosal Immune System Identifies Tissue- and Disease-Associated Immune Subsets. Immunity. 2016;44(5):1227-39.
42. van Unen V, Hollt T, Pezzotti N, Li N, Reinders MJT, Eisemann E, et al. Visual analysis of mass cytometry data by hierarchical stochastic neighbour embedding reveals rare cell types. Nat Commun. 2017;8(1):1740.

43. Beyrend G, Stam K, Hollt T, Ossendorp F, Arens R. Cytofast: A workflow for visual and quantitative analysis of flow and mass cytometry data to discover immune signatures and correlations. Comput Struct Biotechnol J. 2018;16:435-42.

Acknowledgments

We thank Koen Stam and Guillaume Beyrend for the help with statistical analysis of the mass cytometry data, Derk Amsen and Rianne Opstelten for providing the GPA33 antibody for the CyTOF panel and Manou Batstra for determining the autoantibody titres.

Supplementary Materials

Table S1. Antibodies for flow cytometry.

Marker	Fluorochrome	Clone	Dilution
CD19	FITC	4G7	
CD27	FITC	L128	
CD16	PE	B73.1	
HLA-DR	PerCP-Cy5.5	G46-6	
CD127	PerCP-Cy5.5	HIL-7R-M21	
CD25	PE-Cy7	M-A251	
CD28	PE-Cy7	CD28.2	
CD4	APC-Cy7	RPA-T4	
CD8	PB	RPA-T8	
CD3	PB	UCHT1	
CD14	PE-Cy7	61D3	
CD3	APC-Cy7	OKT3	1:500
CD19	PE	HIB19	1:500
CD14	PerCP-Cy5.5	HCD14	1:130
CD16	PE-Cy7	3G8	1:500
CD56	APC	HCD56	1:130
HLA-DR	FITC	LN3	1:500
CD123	BUV395	7G3	1:500
CD11c	BV421	Bu15	1:500
IgD	BV605	IA6-2	1:130
CD27	BUV737	L128	1:130
CD38	BV785	HIT2	1:250
CD24	BV510	ML5	1:250

Table S2. Staining panel for mass cytometry.

Marker	Metal	Clone	Dilution
CD3*	161Dy	UCHT1	1:600
CD4	145Nd	RPA-T4	1:100
CD6*	198Pt	BL-CD6	1:100
CD7	166Er	M-T701	1:800
CD8a	146Nd	RPA-T8	1:800
CD25	169Tm	2A3	1:100
CD27	167Er	O323	1:200
CD28*	171Yb	CD28.2	1:150
CD38	172Yb	HIT2	1:200
CD39*	162Dy	A1	1:100
CD45	89Y	HI30	1:150
CD45RA	Qdot655	MEM-56	1:300
CD49b*	149Sm	P1e6c5	1:50
CD69	144Nd	FN50	1:300
CCR10	138Nd	6588-5	1:40
CD103*	155Gd	Ber-ACT8	1:50
CD107 (LAMP)*	143Nd	H4A3	1:50
CD127	165Ho	AO19D5	1:300
CD152 (CTLA4)*	170Er	14D3	1:40
CD161	164Dy	HP-3G10	1:150
CD138 (CXCR3)	163Yb	G025H7	1:50
CD185 (CXCR5)	173Yb	J252D4	1:100
CD194 (CCR4)*	156Gd	L291H4	1:50
CD196 (CCR6)	141Pr	G034E3	1:100
CD197 (CCR7)	142Nd	G043H7	1:100
CD223 (Lag-3)	150Nd	11C3C65	1:40
CD278 (ICOS)	151Eu	C398	1:50
CD279 (PD-1)	175Lu	EH 12.2H7	1:50
CD357 (GITR)*	159Tb	621	1:40
CD366 (TIM3)	154Sm	F38-2E2	1:50
TIGIT	153Eu	MBSA43	1:50
Putrid (GPA33)*	158Gd		1:50
HLA-DR*	168Er	L243	1:800
LAP (TGF-b)*	174Yb	TW4-2F8	1:40
TCRgd	152Sm	11F2	1:50
KLRG-1*	160Gd	REA261	1:50
GARP*	176Yb	7B11	1:50

*self-conjugated

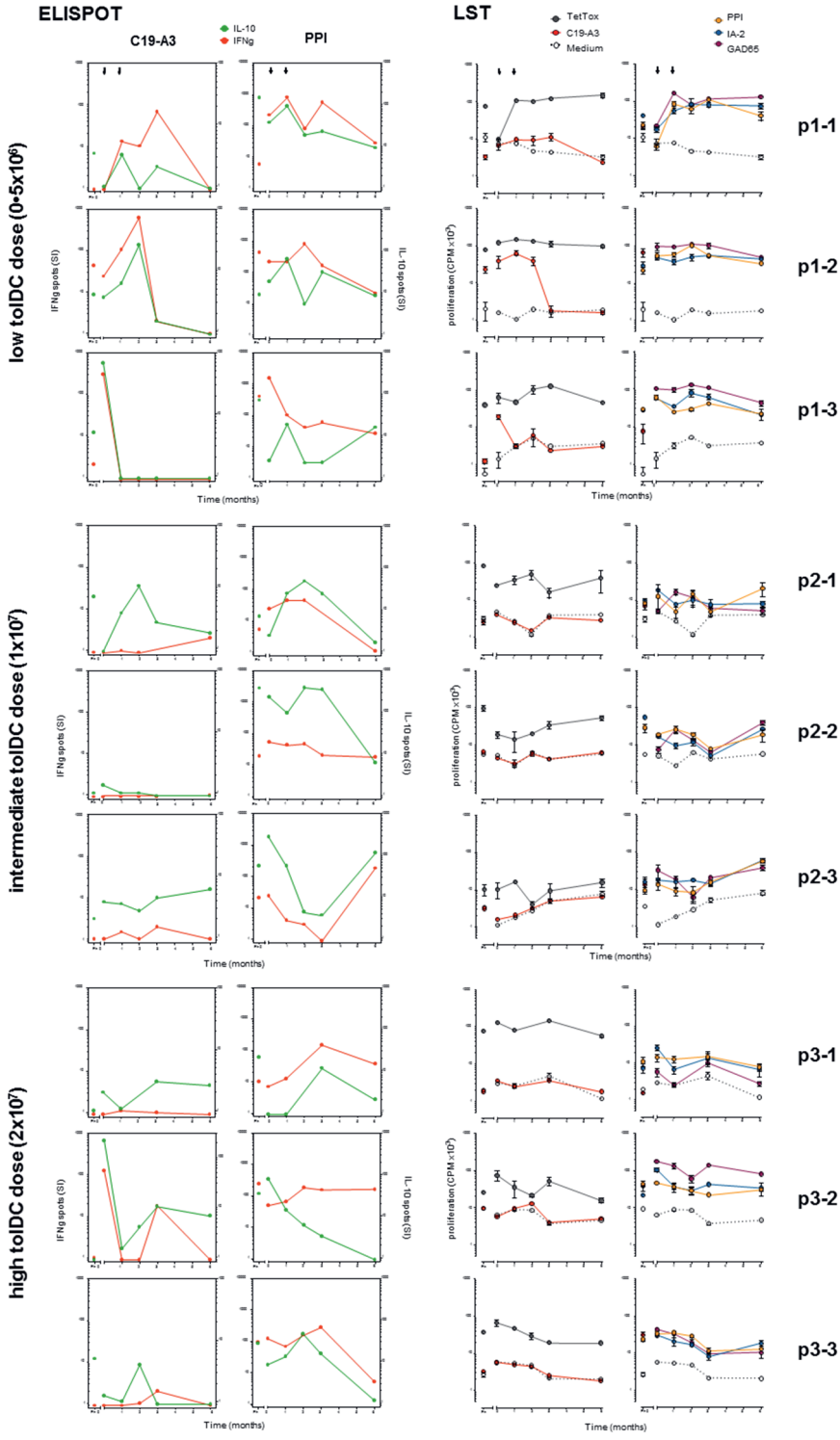
ELISPOT
C19-A3
IL-10
IFNg
PPI
LST
TetTox
C19-A3
Medium
PPI
IA-2
GAD65
low tolDC dose (0•5x10⁶)
intermediate tolDC dose (1x10⁷)
high tolDC dose (2x10⁷)
p1-1
p1-2
p1-3
p2-1
p2-2
p2-3
p3-1
p3-2
p3-3
IFNg spots (SI)
IL-10 spots(SI)
proliferation (CPM x10³)
Time (months)

Fig. S1. Individual patient data for all monitoring timepoints (ELISPOT and LST): prior to leukapheresis (Ph), at tolDC injections (1st = 0; 2nd = 1 month) and at 2, 3 and 6 months after start of tolDC treatment. Arrows in the top row of graphs denote timepoints of tolDC injections. Patient graphs are grouped in panels based on the received tolDC dose (top panel = $5x10^6$; middle panel $10x10^6$; bottom panel $20x10^6$ per tolDC treatment). The left two columns depict cytokine producing cells, expressed in number of spots (green = IL-10 and red = IFNg), specific to the vaccine peptide (C19-A3) or whole proinsulin protein (PPI) as determined by the ELISPOT assay. Right two columns depict T cell proliferation (CPM) as measured by the lymphocyte stimulation test (LST). Red symbols/lines represent proliferation to C19-A3, graey = TetTox, yellow = PPI, blue = IA-2, dark red = GAD65. White symbols with dashed line represent background proliferation without antigen (medium control).

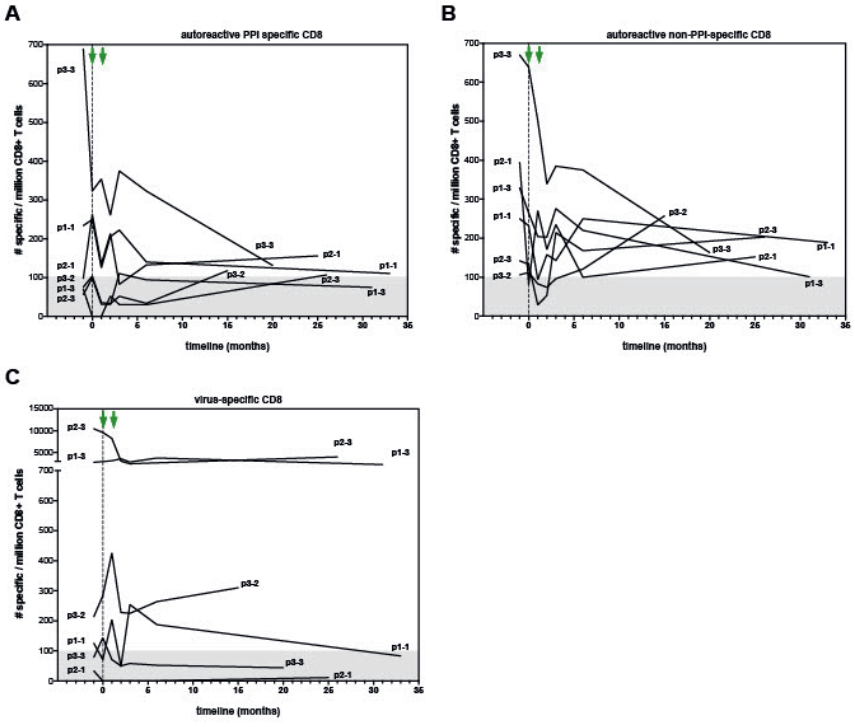

Fig. S2. Q-dot assay for quantification of antigen-specific CD8+ T-cells. (A) Quantification of PPI-specific T-cells (PPI_{15-24}, $InsB_{10-18}$, DRIP) using Q-dot assay prior to leukapheresis (Ph), before tolDC (0) and at different time points after tolDC therapy in six HLA-$A2^+$ patients. In three patients with the highest PPI-specific T-cell counts prior to therapy, reduction after tolDC therapy was observed, while low numbers of PPI-specific $CD8^+$ T-cells pre-treatment, remained low. **(B)** Non-PPI-specific CD8 T-cells reactive to peptides from GAD65, IA-2, IGRP, IAPP and ZnT8 and **(C)** virus-specific specific CD8 T-cells, reacting to CMV, EBV and Measles.

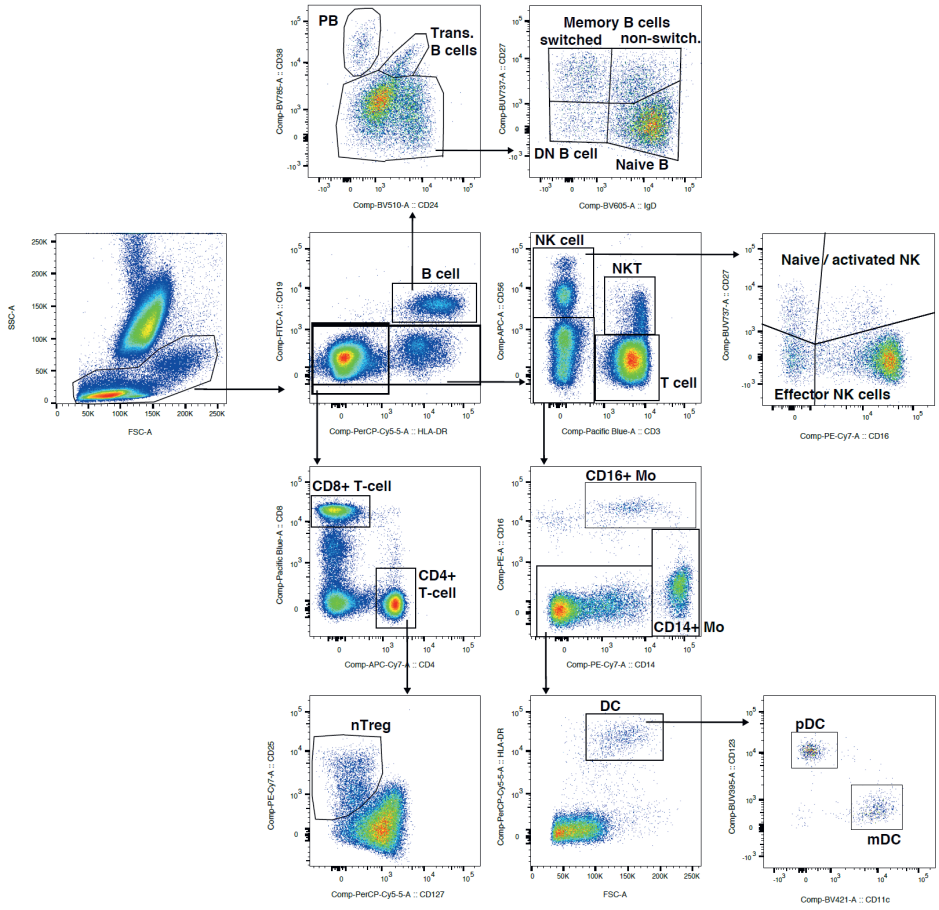

Fig. S3. Gating strategy of flow cytometry data. Major lineages and subpopulations from the innate and adaptive immune system from fresh blood samples are gated for comparison of quantities in time after tolDC treatment (Fig. 4 and Fig. S4).

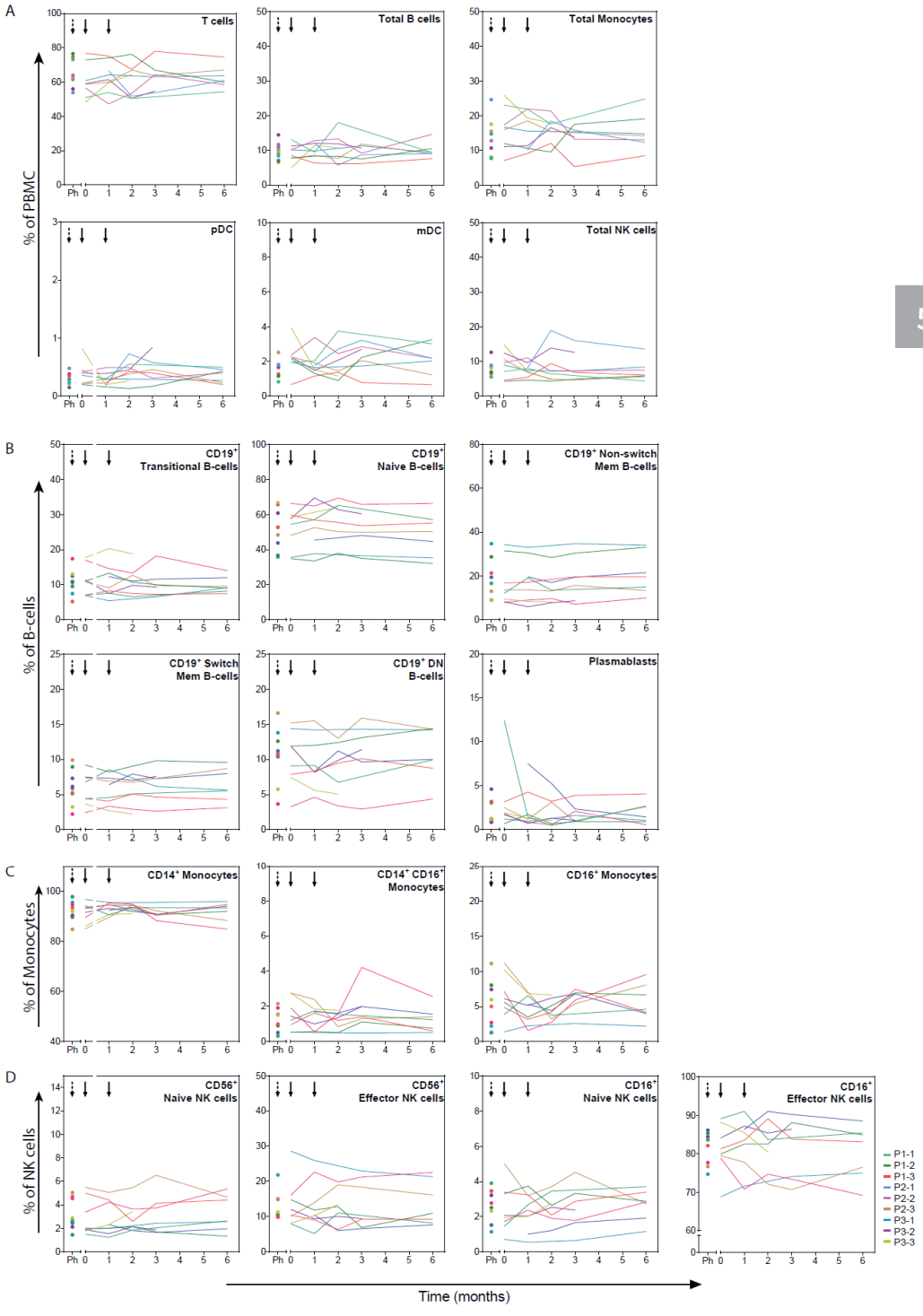
A
% of PBMC
T cells
Total B cells
Total Monocytes
pDC
mDC
Total NK cells
B
% of B-cells
CD19+ Transitional B-cells
CD19+ Naive B-cells
CD19+ Non-switch Mem B-cells
CD19+ Switch Mem B-cells
CD19+ DN B-cells
Plasmablasts
C
% of Monocytes
CD14+ Monocytes
CD14+ CD16+ Monocytes
CD16+ Monocytes
D
% of NK cells
CD56+ Naive NK cells
CD56+ Effector NK cells
CD16+ Naive NK cells
CD16+ Effector NK cells
Ph 0 1 2 3 4 5 6
P1-1
P1-2
P1-3
P2-1
P2-2
P2-3
P3-1
P3-2
P3-3
Time (months)

Fig. S4. Cell frequencies of leukocyte subsets in frozen PBMC. Frequencies determined by flow cytometry. Timepoint before leukapheresis is indicated with black dashed arrow (Ph) and tolDC treatment with black arrows. Line plots show frequencies of **(A)** major immune populations in PBMC **(B)** B-cell subpopulations **(C)** monocyte subpopulations and **(D)** NK cell subpopulations. No significant changes in major immune populations or B-cell/monocyte/NK subpopulations are observed after tolDC injections.

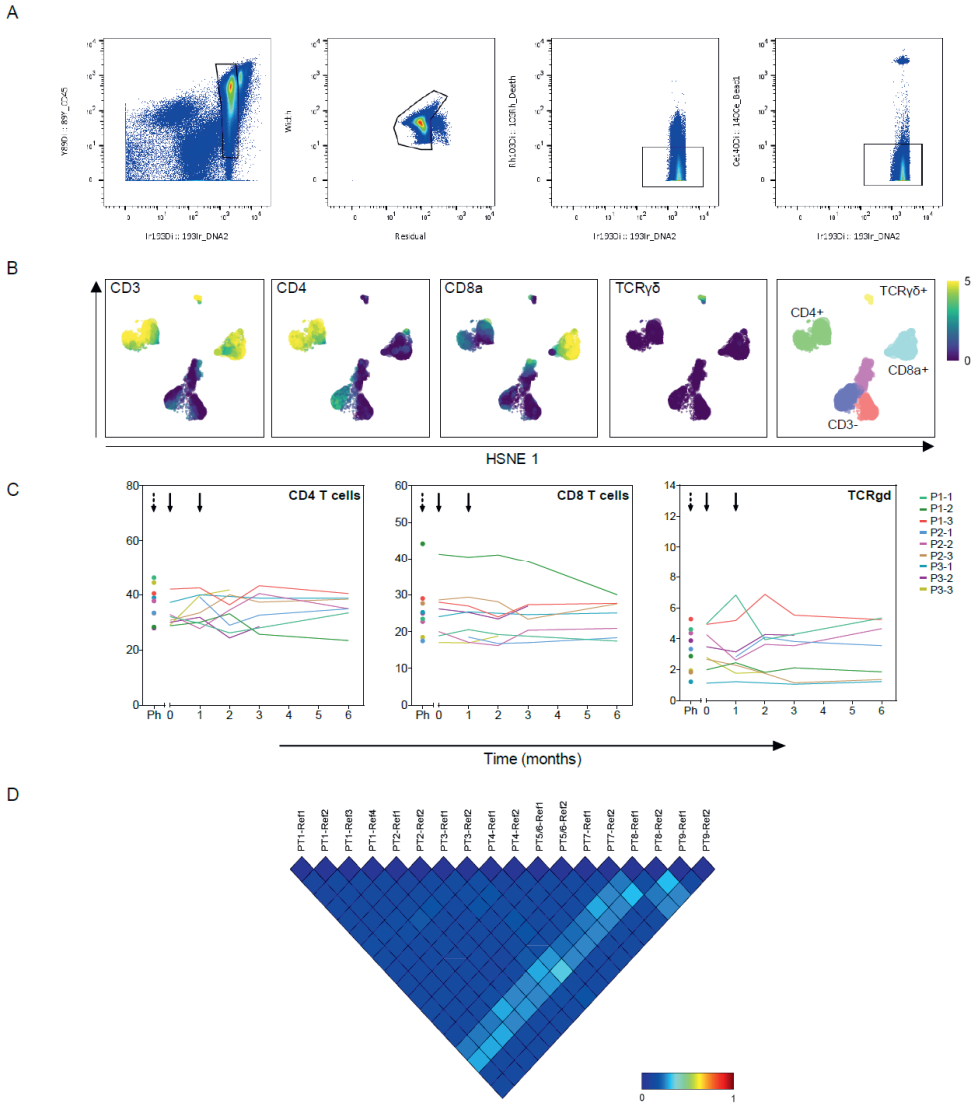

Fig. S5. Gating, high dimensional clustering and quality control of CyTOF dataset. (A) Gating strategy of CyTOF data to select for $CD45^+$ cells. Doublets, dead cells and beads were excluded. **(B)** T-cell populations were identified within $CD45^+$ cells using HSNE analysis. **(C)** Frequencies of $CD4^+$, $CD8^+$ and $TCRgd^+$ T-cells determined with CyTOF analysis, no significant changes after tolDC treatment were observed. **(D)** Jensen-Shannon (JS) plot of reference samples visualizes the consistency of the staining between experiment days. Similarity between tSNE maps of reference samples are measured by the Jensen-Shannon divergence, values are shown between 0 (min) to 1 (max). Per staining, one reference sample was stained alongside the patient samples and subsequently split into different batches to measure at the start and end of each measurement day (1-2).

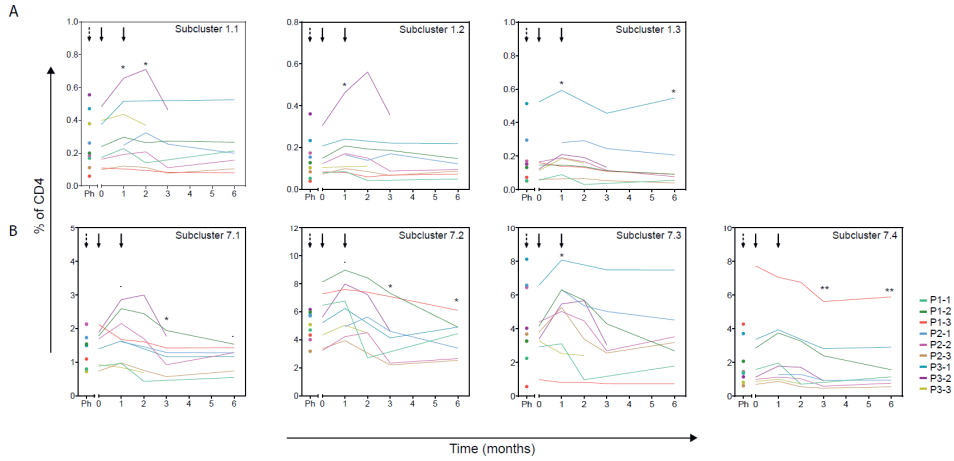

Fig. S6. Line plots of second level CD4⁺ T-cell subclusters that significantly change after tolDC injection. (A) Significant subclusters derived from Trm (CD103⁺) cluster 1 (1.1-1.3) and **(B)** memory cluster 7 with CCR6 expression (7.1-7.4), showing an increase 1 month after the 1st tolDC injection. Subcluster 7.1, 7.2 and 7.4 showed significant decrease after the 2nd tolDC injection compared to baseline frequencies.

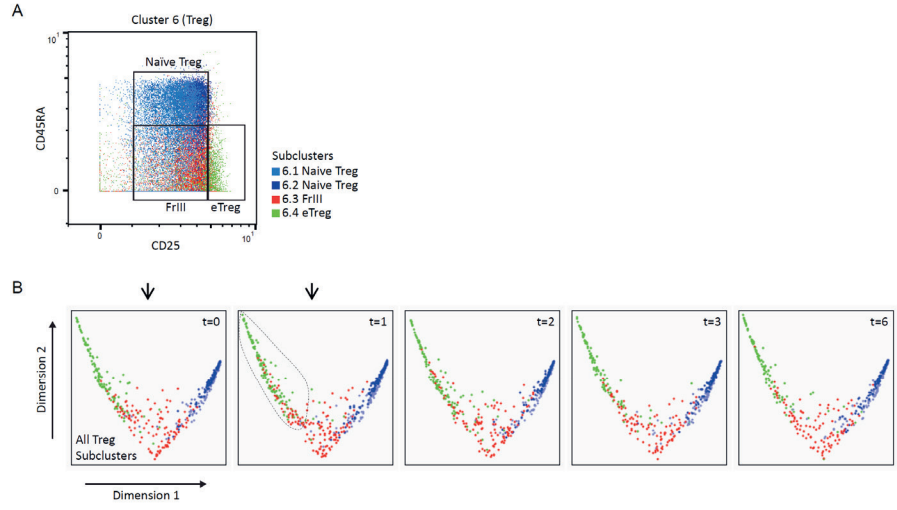

Fig. S7. Second level subclusters of Tregs (A) Treg subclusters as determined by cytosplore visualized in conventional gating view for FACS analysis. **(B)** Diffusion map of Treg cluster 6. Cells from each timepoint are visualized in a different plot. Arrows indicate time of tolDC injection and time is indicated in months.

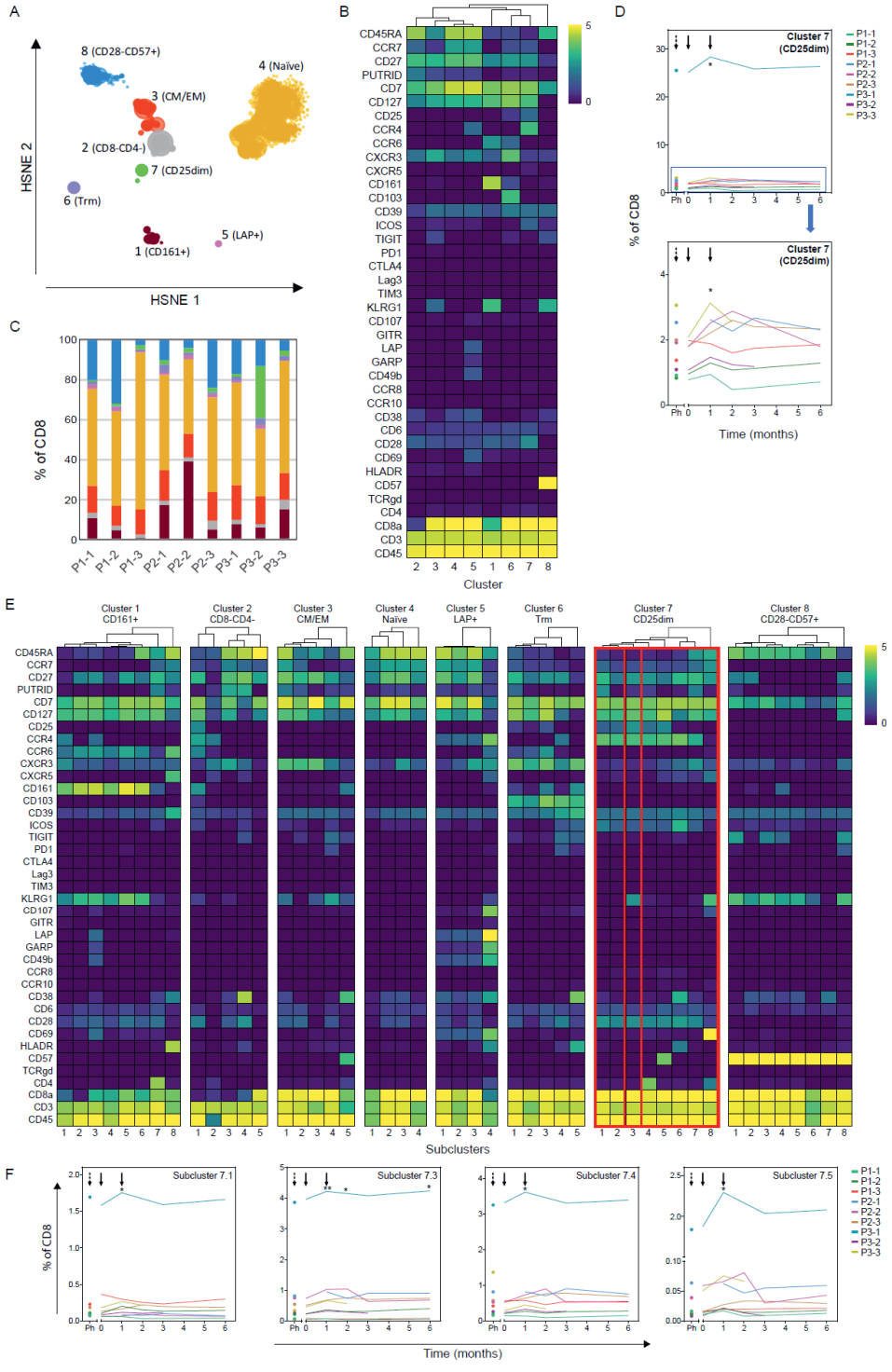
A
8 (CD28-CD57+)
4 (Naïve)
3 (CM/EM)
2 (CD8-CD4-)
7 (CD25dim)
6 (Trm)
5 (LAP+)
1 (CD161+)
HSNE 2
HSNE 1
B
CD45RA
CCR7
CD27
PUTRID
CD7
CD127
CD25
CCR4
CCR6
CXCR3
CXCR5
CD161
CD103
CD39
ICOS
TIGIT
PD1
CTLA4
Lag3
TIM3
KLRG1
CD107
GITR
LAP
GARP
CD49b
CCR8
CCR10
CD38
CD6
CD28
CD69
HLADR
CD57
TCRgd
CD4
CD8a
CD3
CD45
Cluster
C
% of CD8
P1-1
P1-2
P1-3
P2-1
P2-2
P2-3
P3-1
P3-2
P3-3
D
Cluster 7 (CD25dim)
% of CD8
Time (months)
E
Cluster 1 CD161+
Cluster 2 CD8-CD4-
Cluster 3 CM/EM
Cluster 4 Naïve
Cluster 5 LAP+
Cluster 6 Trm
Cluster 7 CD25dim
Cluster 8 CD28-CD57+
Subclusters
F
Subcluster 7.1
Subcluster 7.3
Subcluster 7.4
Subcluster 7.5
% of CD8
Time (months)

Fig. S8. CyTOF analysis of the CD8$^+$ T-cell compartment. Analysis of CD8$^+$ T-cells from different timepoints before and after tolDC treatment (n=9). **(A)** HSNE map of the CD8$^+$ T-cell compartment at the overview level (level 1) shows eight major clusters. **(B)** Heatmap visualizing the phenotype of the major CD8$^+$ T-cell clusters. **(C)** Distribution of major clusters within each patient (all timepoints combined). Colors correspond to clusters represented in the HSNE map in A. **(D)** Line plot of significant cluster 7, showing change in frequency after tolDC injection (p=0.0029). Each line represents one patient and arrows indicate time of tolDC injection. The bottom panel displays a close up of the boxed area in the left panel. **(E)** Heatmap of subclusters of CD8$^+$ T-cells. Boxes indicate significant clusters. **(F)** CD8$^+$ T-cell subclusters that significantly change after tolDC injection. Arrows indicate time of tolDC injection and each line represents one patient.